THE JOURNAL OF PHYSICAL CHEMISTRY A

 VOLUME 106, NUMBER 2, JANUARY 17, 2002

ARTICLES

Equilibrium and Dynamical Aspects of Solvation of Coumarin-151 in Polar Nanoclusters

Alejandro Tamashiro,[†] Javier Rodriguez,[†] and Daniel Laria*[,†,‡]

Unidad Actividad Química, Comisión Nacional de Energía Atómica, Avenida Libertador 8250, 1429 Buenos Aires, Argentina, and Departamento de Química Inorgánica, Analítica y Química-Física e INQUIMAE, Facultad de Ciencias Exactas y Naturales, Universidad de Buenos Aires, Ciudad Universitaria, Pabellón II, 1428 Buenos Aires, Argentina

Received: July 10, 2001; In Final Form: October 22, 2001

Molecular dynamics experiments have been performed to study equilibrium aspects of the solvation of Coumarin-151 in polar nanoclusters containing $N_s = 5$, 10, and 50 water and methanol molecules. In small aggregates, both solvents show preferential solvation of the amino group of the solute. Whereas in aqueous aggregates the dye molecule shows a propensity to reside on the cluster surface for all sizes investigated, the 50 methanol cluster exhibits clear signs of more uniform, bulklike solvation. Using nonequilibrium simulations, we also studied the solvation dynamics upon an electronic excitation of the probe. At temperatures close to $T = 200$ K, small clusters exhibit two well differentiated equilibrium solvation structures for the excited states of the solute. Interconversions between these structures take place in a time scale much longer than the one characterizing the solvation relaxation. In $N_s = 5$ clusters, the nonequilibrium responses are exclusively dominated by a fast inertial relaxation lasting less that 0.1 ps; for $N_s = 50$, the relaxations exhibit a slow diffusional regime that dominates the long time behavior as well. The overall response of the largest clusters is also analyzed in terms of linear response theories.

I. Introduction

The study of equilibrium and dynamical aspects of chemical reactivity in polar nanoclusters presents distinctive features that are normally absent in conventional macroscopic phases.[1−3] Perhaps the most important reasons that account for these peculiarities are to be found in the lack of translational symmetry and in the presence of a free surface nearby that lead to large anisotropies in the microscopic forces fields exerted on the different cluster constituents. In small and intermediate size aggregates, these effects are translated into strong spatial and orientational correlations that, in turn, affect the different reaction pathways. The solvation structures and dynamics of molecular probes in nanoclusters are also strongly influenced by the interplay between surface and bulk forces, which is clearly manifested in the stabilization of surface or cluster−interior solvated species.[4] These are some of the issues that will be investigated in this paper.

Our motivation focuses on establishing similarities and differences between several aspects of solvation in bulk polar phases and in their counterparts at the nanometer scale. Spurred by a series of recent infrared spectroscopy studies by Topp et al.,[5−7] we examined equilibrium and dynamical aspects of the solvation of Coumarin-151 (C-151) attached to water and methanol clusters containing up to 50 molecules using molecular dynamics techniques. C-151 (7-amino-4-trifluoromethylcoumarin) is a polycylcic aromatic dye particularly suitable for

* To whom correspondence should be addressed. E-mail: dhlaria@cnea.gov.ar.
[†] Comisión Nacional de Energía Atómica.
[‡] Universidad de Buenos Aires.

10.1021/jp012626x CCC: $22.00
Published on Web 12/14/2001

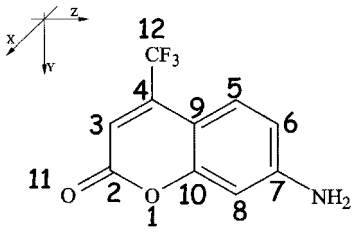

Figure 1. Coumarin-151.

studying polar solvation because of its dual role as potential proton donor/acceptor via the amino/carbonyl groups (see Figure 1). From the analysis of the different vibrational bands, Topp et al. were able to distinguish preferential solvation between these two groups and, in certain cases, the simultaneous presence of isomers with well differentiated solvation structures for the same cluster species.[6,7]

The characterization of bulk polar solvation of relatively large polyatomic solutes such as C-151 is not always straightforward given the wide variety of length scales involved in the problem. These length scales are associated with the particular charge distribution of the solute and the specifities of the solute−solvent and solvent−solvent interactions, with all of them of similar magnitude. The absence of a clear separation between these parameters precludes a simple analysis based, for example, on the examination of the different solvent density fields around the probe. Interpretation of the solvation in nanoclusters is even more complex, given the effects imposed by the spatial confinement that prevails in these aggregates. In a much wider context, the problem bears several aspects in common with solvation in other microheterogeneous structures such as interfaces[8] or complex bioenvironments[9,10] where the properties of the solvent differ drastically from what is known in bulk phases. Within this framework, computer simulation experiments emerge as one of the most suitable tools to gain a realistic insight on the microscopic details of the gradual changes that take place in the solvation as we move from isolated molecule states to macroscopic phases.

Coumarins are also very popular as molecular probes to monitor ultrafast dynamical aspects of solvation via time-resolved Stokes shift experiments. An exhaustive enumeration of previous experimental and theoretical work in this area is well beyond the scope of this work, so we will refer the interested reader to a few recent review articles.[11−17] The dynamical characteristics of polar solvation in bulk phases are sufficiently well established; a distinctive characteristic of the overall response of these environments is given by its bimodal character, i.e., an initial fast transient accounting for a major fraction of the total response and lasting a few hundreds of femtoseconds, followed by a much slower diffusive regime with characteristic time scale of the order of 1−5 ps. In this work, we also shed light on the dynamical characteristics of the response of different clusters upon an electronic excitation of C-151 by trying to establish a correspondence between the different relaxation mechanisms and the limiting, initial and final, equilibrium solvation structures.

The remainder of this paper is organized as follows: In section II, we provide details of the model and the methodology implemented in the simulation runs. Results for the nonequilibrium responses are presented in section III. Section IV includes an analysis of the equilibrium solvation structures. An interpretation of the overall responses in terms of microscopic mechanisms is provided in section V. Concluding remarks are presented in section VI.

II. Model

The systems under investigation were composed by a single C-151 dissolved in polar clusters containing N_s molecules of solvent ($s = H_2O$ or MeOH). All molecules were modeled as a collection of sites kept at fixed distances. Coumarin−solvent (U_{cs}) and solvent−solvent (U_{ss}) potential energies were considered as a sum of site−site Lennard-Jones plus Coulomb interactions.

The molecular geometry and charge distributions of C-151 were computed using the AM1 parametrization of the semiempirical AMPAC package.[18] This parametrization is known to provide reasonable descriptions of the electronic densities of several coumarin dyes.[19−21] A full geometry optimization for the C-151 ground state, S_0, was performed using a restricted Hartree−Fock closed shell algorithm. The excited state, S_1, was constructed by performing a configuration interaction (CI) calculation with 100 microstates at the ground-state optimized geometry. These many states were used in order to achieve convergence of the CI energy with respect to the number of microstates within 1.0 kcal/mol and are believed to provide a fair approximation of correlation effects. An analysis based on the Mulliken populations was implemented in order to obtain a charge value for the different atomic sites in both ground and excited states. Our calculations yielded values $\mu_{S_0} = 5.7$ and 11.0 D for the dipole moment; these results are in reasonable agreement with previous calculations.[19,20]

To describe the geometry and charge distribution of the water molecule, the simple point charge model by Berendsen et al.[22] was adopted. A similar description was used for the MeOH molecule, which comprised three interaction sites O, H, and the united atom model for CH_3.[23] Full details of the parameters for the solute and solvent interactions can be found in Table 1.

The dynamical trajectories corresponded to microcanonical runs at temperatures close to $T \approx 200$ K; in this thermal regime, all systems exhibited dynamical, liquidlike behavior with negligible evaporation during the course of the simulation runs.[24] Three cluster sizes were investigated, $N_s = 5$, 10, and 50. Statistics were collected over rather long equilibrium trajectories lasting typically ≈5 ns. Nonequilibrium runs were performed by first selecting initial 1000 conditions from a previous equilibrium run, separated by 5 ps intervals to provide statistically independent configurations. From these initial conditions, we monitored the relaxations of relevant observables during typical periods of 5 ps. The Verlet algorithm[25] was employed to integrate the equations of motion with a time step of 1 fs. Intramolecular constraints were treated using the SHAKE algorithm.[26]

III. Nonequilibrium Solvation

We are interested in describing the dynamics of cluster solvation following a vertical electronic excitation of C-151. The simplest way to tackle the problem is by considering the normalized nonequilibrium response defined by

$$S(t) = \frac{\langle E(t) - E(\infty)\rangle_{ne}}{\langle E(0) - E(\infty)\rangle_{ne}} \tag{1}$$

In the previous equation, $\langle ... \rangle_{ne}$ denotes an average taken from a distribution of nonequilibrium initial configurations.[27] $E(t)$ is the instantaneous Coulombic energy gap[21]

$$E(t) = \sum_{\alpha} E_{\alpha}(t) = \sum_{\alpha} \Delta q_{\alpha} V_{\alpha}(t) \tag{2}$$

TABLE 1: Parameters for the Potentials

A. Solvents

site	σ	ϵ	q
	H_2O		
O	3.17	0.156	−0.82
H	0.00	0.000	0.41
$d_{O-H} = 1.0$ Å; $d_{H-H} = 1.633$			
	MeOH		
O	3.071	0.170	−0.700
H	0.000	0.000	0.435
CH_3	3.775	0.207	0.265
$d_{O-CH_3} = 1.424$; $d_{O-H} = 0.9451$; $d_{CH_3-H} = 1.943$			

B. Coumarin-151

					c_α	
site	σ^a	ϵ^a	q_α	Δq_α	$N_{H_2O} = 50$	$N_{MeOH} = 50$
C_2			0.332	−0.027	0.044	0.042
C_3			−0.191	−0.080	0.184	0.188
C_4			−0.035	−0.228	0.440	0.356
C_5			−0.025	−0.054	−0.041	−0.032
C_6			−0.211	0.079	0.140	0.139
C_7	3.50	0.080	0.147	−0.066	−0.140	−0.156
C_8			−0.240	0.082	0.123	0.141
C_9			−0.179	0.212	−0.066	−0.035
C_{10}			0.145	−0.024	−0.007	−0.011
C_{12}			0.460	−0.004	0.006	0.007
O_1	2.96	0.210	−0.186	−0.013	0.008	0.004
O_{11}			−0.273	0.012	−0.016	−0.018
N	3.25	0.170	−0.349	0.124	0.313	0.361
F[b]	2.80	0.105	−0.157	−0.004	0.002	0.003
H	2.50	0.005	0.14−0.21[c]	0.000	0.000	0.000

[a] The Lennard Jones parameters were considered the same for the S_0 and the S_1 states. [b] The three F sites have identical parameters. [c] The values represent the minimum and maximum values for the partial charges of the H sites. Length parameters are given in Å; energy parameters are given in kcal/mol; charge parameters are given in e. The usual geometrical and arithmetic means were used to determined the ϵ and σ parameters for the cross interactions.

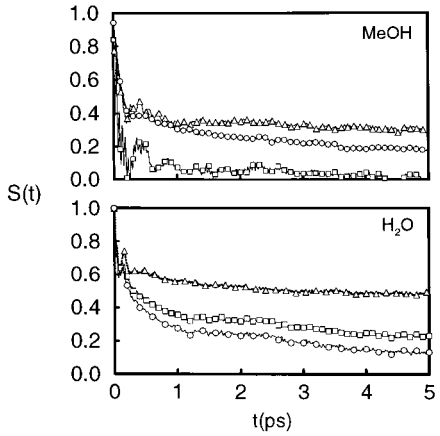

Figure 2. Solvation responses for different polar clusters containing N_s solvent molecules. Triangles, $N_s = 5$; squares, $N_s = 10$; circles, $N_s = 50$.

where Δq_α and $V_\alpha(t)$ represent the charge jump and the instantaneous solvent electrical potential at the α site of C-151 at time t, respectively.

In Figure 2, we present results for the solvation relaxations. Notwithstanding the obvious differences in intermolecular interactions and sizes, at a first glance, the six curves look qualitatively rather similar. However, a closer inspection of the top and bottom panels reveals peculiarities in the individual behaviors which are worth commenting. We start by considering the particularly intriguing results for the smallest aggregates: note that the dynamical responses exhibit an unusually slow

TABLE 2: Solvation Parameters for Different Polar Clusters

	N_s	$\tau_s{}^a$	$\tau_s{}^b$	$\langle E(0)\rangle$	$\langle E(\infty)\rangle^a$	$\langle E(\infty)\rangle_{\mathcal{A}}$	$\langle E(\infty)\rangle_{\mathcal{B}}$
	5	>30[c]	0.5	−1.1	−3.7	−2.5	−4.3
H_2O	10	3.7	1.6	−1.9	−5.8	−5.4	−6.1
	50	1.7	1.7	−2.3	−6.9		
	5	>10[c]	0.28	−2.2	−3.4	−3.0	−5.7
MeOH	10	0.3	0.3	−3.9	−5.1		
	50	3.7	3.7	−2.5	−7.0		

[a] Computed from 5 ns equilibrium runs and assuming that $S(t)$ presents a single-exponential decay for $t > 5$ ps. [b] Computed from an equilibrium average taken exclusively over state $\mathcal{A}$ (see text). [c] The errors in the long time portion of the correlation are too large to obtain a more precise estimation. Energies are given in kcal/mole, and times are given in ps.

decay. After a short transient lasting ≈100 fs, the curves for both solvents seem to level off at practically plateau values of the order of $S(t) \simeq 0.4-0.5$. A crude estimate of the overall characteristic relaxation time, τ_s, can be obtained from the integral

$$\tau_s = \int_0^\infty S(t)\, dt \qquad (3)$$

Results for τ_s are displayed in the third column of Table 2 where one can see that for $N_s = 5$ both τ_s surpass 30 ps! Another puzzling result is given by the fact that, although water clusters exhibit a monotonic τ_s vs size dependence, the fastest relaxation for methanol clusters corresponds to the intermediate size aggregate, $\tau_s = 0.3$ ps for $N_{MeOH} = 10$. The two examples

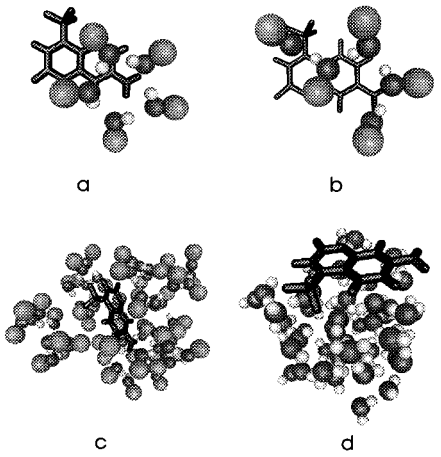

Figure 3. Snapshots for typical configurations for clusters containing the probe C-151. (a) $N_{MeOH} = 5$ (S_0 solute); (b) $N_{MeOH} = 5$ (S_1 solute, state $\mathscr{B}$); (c) $N_{MeOH} = 50$ (S_0 solute); (d) $N_{H_2O} = 50$ (S_0 solute).

that we have just presented reveal important qualitative differences and a wide variety of time scales whose rationalization will require a more detailed analysis in terms of temporal and spatial correlations that we will perform in the next sections.

IV. Equilibrium Solvation Structures

Before addressing the dynamical aspects of solvation, it will be instructive to briefly digress on the equilibrium solvation structures for the different cluster sizes. In Figure 3, we present snapshots of typical cluster configurations. For the smallest clusters, the solvation structures are practically identical for both solvents and are characterized by a highly asymmetric distributions localized in the vicinity of the amino group. The degree of asymmetry can be described in terms of the angular distributions n_1 and n_2 defined as

$$n_1[\cos(\theta)] = \frac{1}{N_s}\sum_{i=1}^{N_s}\langle\delta[\cos(\theta_i) - \cos(\theta)]\rangle$$

$$n_2(\phi) = \frac{1}{N_s}\sum_{i=1}^{N_s}\langle\delta(\phi_i - \phi)\rangle \qquad (4)$$

where θ_i and ϕ_i identify the angular coordinates of the center of mass of the ith solvent molecule with respect to the local coordinate system with the origin at the solute center of mass, also shown in Figure 1. Results for the angular correlations are displayed in Figure 4. We observe that the n_1 distributions are peaked at $\cos(\theta) \approx 0.8$, revealing the preferential solvation of the amino group located at $\cos(\theta_{NH_2}) = 0.92$. The n_2 distributions show two zones of preferential solvation at $\phi \approx \pi/4$ and $\phi \approx 3\pi/4$ with less favorable configurations exhibiting $\phi = \pi/2$; given that the site distribution of the molecule of C-151 lies practically on the $x = 0$ plane, these results suggest the presence of free energy barriers (somewhat higher for MeOH than for H_2O) that prevent frequent solvent transitions from $x > 0$ to $x < 0$ regions.

The scenarios for the largest clusters contrast sharply (see snapshots c and d of Figure 3): although in the aqueous aggregate the solute still exhibits surface states, solvation in 50 MeOH presents clear signs of internal, "bulklike" behavior. These two structures can be conveniently described in terms of three correlations functions: first, the spatial correlations between the

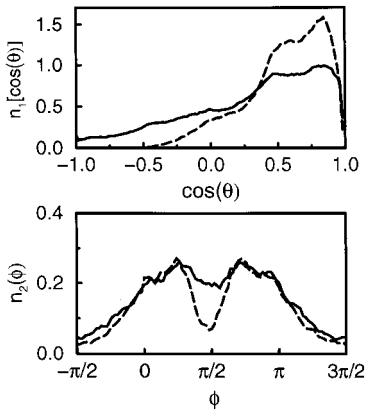

Figure 4. Angular distributions for the solvation in $N_s = 5$ clusters (see text). Solid lines, H_2O; dashed lines, MeOH.

center of mass of the coumarin, $\boldsymbol{R}_c$, and the center of mass of the solvent, $\boldsymbol{R}_s$, defined as

$$g_{cs}(r) = \frac{1}{4\pi r^2}\langle\delta(|\boldsymbol{R}_c - \boldsymbol{R}_s| - r)\rangle \qquad (5)$$

second, the spatial correlation between the individual solvent molecules and $\boldsymbol{R}_s$, namely

$$g_s(r) = \frac{1}{N_s 4\pi r^2}\sum_{i=1}^{N_s}\langle\delta(|\boldsymbol{R}^i_{CM} - \boldsymbol{R}_s| - r)\rangle \qquad (6)$$

where $\boldsymbol{R}^i_{CM}$ denotes the coordinate of the center of mass of the ith solvent molecule; and finally, a third distribution, $P[\cos(\theta)]$, that provides information about the orientation of C-151 at the water cluster surface

$$P[\cos(\theta)] = \langle\delta[\cos(\theta_{cs}) - \cos(\theta)]\rangle$$

$$\cos(\theta_{cs}) = \frac{\hat{\boldsymbol{x}}\cdot(\boldsymbol{R}_c - \boldsymbol{R}_s)}{|\boldsymbol{R}_c - \boldsymbol{R}_s|} \qquad (7)$$

where $\hat{\boldsymbol{x}}$ is a versor in the x direction of the local coordinate system. In Figure 5, we present results for these distributions. From the simultaneous analysis of the three sets of curves, one can conclude that the most probable solvation structure in the aqueous aggregate corresponds to the C-151 with its molecular plane mostly tangential to the cluster surface at a distance $\approx$7.5 Å from the $\boldsymbol{R}_s$. On the other hand, in the 50 MeOH cluster, the coumarin lies practically at the center of mass of the aggregate and the solvent density profile presents a much more inhomogeneous and less compact structure compared to that of its water counterpart. We refrain from commenting on the solvation structures for S_1 solutes because they present similar qualitative characteristics to those already described for the S_0 cases.

V. Solvation Dynamics

Having established the main features of the equilibrium solvation structures, we now turn to the dynamical analysis of the solvation. We start by trying to unveil the origin of the slow decay that dominates the long time regime of the smallest cluster responses. In Figure 6, we present results for the time evolution of $E(t)$ along two long equilibrium runs with S_0 and S_1 solutes. The differences in the two sets of curves are noteworthy: although S_0 curves are characterized by fast ($\approx$50 fs) oscillations around their average values, both S_1 curves exhibit a distinctive

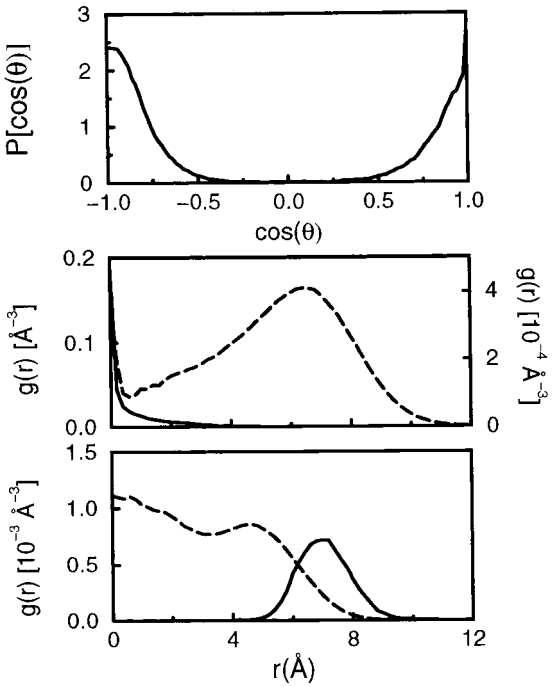

Figure 5. Angular and spatial correlation for C-151 dissolved in $N_s = 50$ clusters. Top panel: angular correlation for the superficial orientation of the solute attached to a 50 H_2O cluster. Middle panel: pair correlation functions $g_{cs}(r)$ (solid line, left axis) and $g_s(r)$ (dashed line, right axis) for $N_{MeOH} = 50$ cluster (see text). Lower panel: same as in the middle panel for an $N_{H_2O} = 50$ cluster.

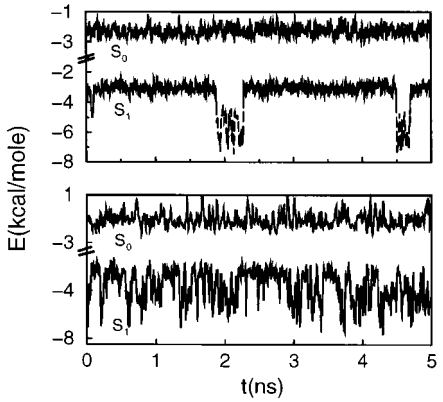

Figure 6. Top panel: time evolution of the solvent energy gap $E(t)$ for the S_0 and the S_1 states of C-151 attached to an $N_{MeOH} = 5$ cluster. Configurations corresponding to $\mathscr{A}$ and $\mathscr{B}$ states in the S_1 trajectory are plotted in solid and dash lines, respectively. Bottom panel: same as the top panel for an $N_{H_2O} = 5$ cluster.

bimodal character. The particular case of the methanol cluster is perhaps the clearest: one can identify two episodes, at $t =$ 1.8 and 4.45 ns, corresponding to sudden transitions between two solvation states, hereafter referred to as states $\mathscr{A}$ and $\mathscr{B}$, respectively. These states are characterized by average gaps $\langle E\rangle_{\mathscr{A}} \approx -3.0$ kcal/mol and $\langle E\rangle_{\mathscr{B}} \approx -5.6$ kcal/mol; a similar analysis performed on the time evolution of the different couplings shows that state $\mathscr{A}$ presents stronger solvent−solvent interactions ($\langle U_{ss}\rangle_{\mathscr{A}} = -39.4$ kcal/mol and $\langle U_{ss}\rangle_{\mathscr{B}} = -30.5$ kcal/mol) and weaker solvent−solute interactions ($\langle U_{cs}\rangle_{\mathscr{A}} = -6.2$ kcal/mol and $\langle U_{cs}\rangle_{\mathscr{B}} = -12.7$ kcal/mol). The solvation structure of state $\mathscr{A}$ looks practically identical to that already described in the previous paragraph for S_0 solutes (see Figure 3a). On the other hand, in state $\mathscr{B}$, the solvent stretches across the solute molecule generating a "chain structure" bridging the distal amino group

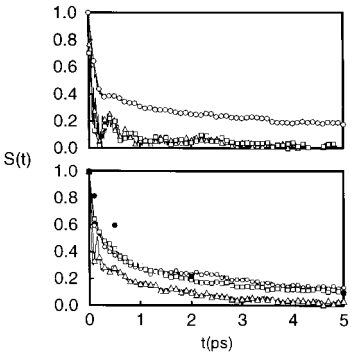

Figure 7. Solvation responses for different polar clusters considering $\langle E(\infty)\rangle_{ne} = \langle E\rangle_{\mathscr{A}}$ (see text). Same labeling as in Figure 2. Also shown is the nonequilibrium relaxation of ΔN_H for the $N_{H_2O} = 50$ cluster (black circles).

to the central part of the coumarin (see Figure 3b). Note that it is in this region where the largest changes in Δq_α take place (see Table 1B), and this might provide an explanation for the absence of solvation structures of type $\mathscr{B}$ for S_0 solutes. A similar situation is found in small water clusters; however, the time scale for the interconversion drops to a few tens of picoseconds (see the lower panel of Figure 6) revealing a much lower activation free energy for the transitions.

The presence of two decorrelation time scales for the temporal dependence of $E(t)$ in the S_1 case, one on the order of a few picoseconds and a second one at least 3 orders of magnitude larger, provides some clues to explain the unusually long relaxation of $S(t)$: we have verified that the solvation structures during the first picoseconds after the vertical excitation correspond exclusively to state $\mathscr{A}$. Under these circumstances, the clear separation of time scales suggests that the interconversion between $\mathscr{A}$ and $\mathscr{B}$ can be treated as an independent, much slower process, totally uncorrelated to the initial relaxation of the solvation structure. Of course, this peculiarity is a finite size effect that should progressively be less important as the size of the aggregates and that of the solute become comparable. At this point, an important question arises, namely, which value should be included in eq 1 for the limiting value $\langle E(\infty)\rangle_{ne}$. Results shown in Figure 2 correspond to averages taken over the complete 5 ns trajectory, namely, $\langle E(\infty)\rangle_{ne} = -3.7$ and -3.4 kcal/mol for water and methanol clusters, respectively. In Figure 7, we present results for the same relaxations as those shown in Figure 2 but now assuming that $\langle E(\infty)\rangle_{ne} = \langle E\rangle_{\mathscr{A}}$. Note that with this choice a similar monotonic τ_s vs size dependence is recovered for both solvents (see the fourth column of Table 2), with the smallest clusters presenting the fastest relaxations with practically exclusive inertial characteristics.

We now turn to the analysis of the slower diffusive regime of the response in the largest clusters. Because in our model the details of the electronic density of the probe are incorporated via a discrete distribution of point charges, it will useful to decompose the total response in terms of a weighted sum of different solute-site contributions $S_\alpha(t)$, namely

$$S(t) = \sum_\alpha c_\alpha S_\alpha(t) \tag{8}$$

where

$$S_\alpha(t) = \frac{\langle E_\alpha(t) - E_\alpha(\infty)\rangle_{ne}}{\langle E_\alpha(0) - E_\alpha(\infty)\rangle_{ne}} \tag{9}$$

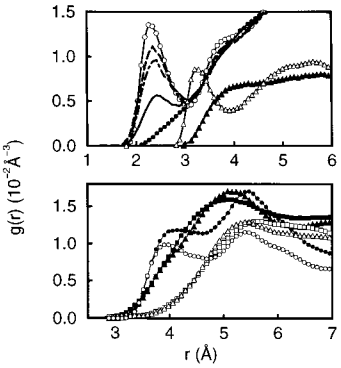

Figure 8. C_4-solvent pair correlation functions for N_s clusters. Top panel, H_2O; triangles, g_{C_4-O}; circles, g_{C_4-H}. The full and open symbols correspond to S_0 and S_1 solutes, respectively. Also shown is the nonequilibrium g_{C_4-H} at selected times: $t = 0.5$ ps, dotted lines; $t = 2$ ps, dot−dashed lines; $t = 5$ ps, dashed lines. Bottom panel: MeOH; triangles, g_{C_4-H}; circles, $g_{C_4-CH_3}$; squares, g_{C_4-O}.

In eq 8, the weight c_α represents the fractional contributions of site α to the total Coulomb energy gap:

$$c_\alpha = \frac{\langle E_\alpha(0) - E_\alpha(\infty)\rangle_{ne}}{\langle E(0) - E(\infty)\rangle_{ne}} \tag{10}$$

The results shown in columns 4 through 7 of Table 1B reveal several interesting features:

(i) The largest changes in the electronic distribution of the probe take place in two central carbon sites, where there is a transfer ≈ −0.20 e from C_9 into C_4, and in the N site, Δq_N = 0.12 e.

(ii) the values of c_α appear to be only partially correlated to Δq_α. For instance, although the C_4 and N weights account for almost 80% of the total solvent-energy gap, the magnitude of the c_α for the central C_9, with the second largest charge jump, represents only a ≈5% of the total solvent gap.

(iii) Yet, more interestingly, note that contributions from some selected solute sites, including the aforementioned C_9, are negative, revealing that the total response is the result of partial cancellations between different site relaxations. The physical picture that emerges from these observations suggests that the solvent electric field is not sufficiently quickly variant in space so as to provide simultaneous stabilization to solute sites with opposite Δq_α lying at very small separations.

A microscopic interpretation of the diffusive regime normally requires the study of the transients of different density solvent fields in the vicinity of the probe; previous simulation studies reveal that the dynamics of ionic solvation is basically dominated by the contribution from closest solvent shells.[28] We shall focus our attention exclusively on the solute−solvent spatial correlations for the central C_4, which is the site that exhibits the largest c_α and analyze different radial distribution functions, defined as

$$g_{\alpha\gamma}(r;t) = \frac{1}{4\pi r^2}\sum_{j=1}^{N_s}\langle\delta(|\boldsymbol{r}_\alpha(t) - \boldsymbol{r}^j_\gamma(t)| - r)\rangle_{ne} \tag{11}$$

where $\boldsymbol{r}_\alpha(t)$ and $\boldsymbol{r}^j_\gamma(t)$ refer to the coordinates of site α = C_4 of the coumarin and the γ site of the *j*th solvent molecule at time *t*, respectively. In the top panel of Figure 8, we present results for the limiting $t = 0$ (S_0) and ∞ (S_1) equilibrium states for 50 H_2O clusters; in addition, nonequilibrium spatial correlations for the H site of the solvent collected at three intermediate times along the relaxation process are included as well. The sudden build up of negative charge at the solute site promotes the gradual formation of two peaks: one in g_{C_4-H} at $r = 2.2$ Å and a second one in g_{C_4-O} at $r = 3.2$ Å, both with similar area at $t = \infty \approx 0.9$. Moreover, in Figure 7, we also included results for the ratio

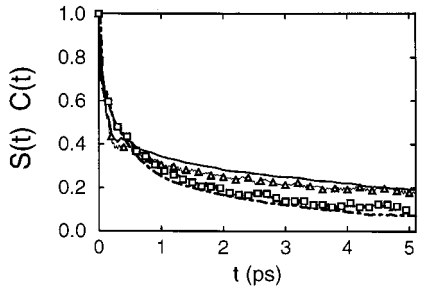

Figure 9. Equilibrium and nonequilibrium time correlation functions of the solvent energy gap in $N_s = 50$ clusters. Triangles, $C(t)$ for MeOH; squares, $C(t)$ for H_2O; solid line, $S(t)$ for MeOH; dot−dashed line, $S(t)$ for H_2O.

$$\Delta N_H(t) = \frac{\langle N_H(t) - N_H(\infty)\rangle_{ne}}{\langle N_H(0) - N_H(\infty)\rangle_{ne}} \tag{12}$$

where N_H represents the integral under the first peak of g_{C_4-H}. The almost perfect agreement between the $S(t)$ curve and the relaxation of $\Delta N_H(t)$ would be indicative of the diffusive character of the local solvent response in the vicinity of the tagged solute site, involving a disruption of the original cluster surface structure as a consequence of the breaking of a water−water hydrogen bond, the approach of a water molecule toward the solute site, and the subsequent formation of a new linear $C_4\cdots H-O$ bond. C_4-solvent spatial correlations for 50 MeOH clusters show no signs of new bonds (see bottom panel of Figure 8); moreover, upon excitation, the different profiles suffer overall changes in the opposite direction to that described for water, with a significant loss of structure in the neighborhood of the tagged solute site.

Before closing this section, we will comment on a last aspect dealing with the validity of linear response theory (LRT) to describe the nonequilibrium relaxations. Using Onsager's regression hypothesis and for sufficiently small perturbations, the relaxation of $S(t)$ can be reasonably well approximated by the equilibrium correlation function $C(t)$:[27]

$$S(t) \approx C(t) = \frac{\langle\delta E(t)\,\delta E(0)\rangle}{\langle(\delta E)^2\rangle} \tag{13}$$

where $\delta E(t) = E(t) - \langle E\rangle$. LRT has proven to be a robust and successful tool to predict the main features of the time evolution of solvation response of a large variety of polar and nonpolar environments, even for solvent energy gaps much larger than the usual thermal energies involved in the systems. However, a singular behavior was observed in bulk methanol, where the theory was found to work rather poorly.[29] Therefore, we felt it important to test if these inadequacies still persist in cluster environments. The performance of LRT for the largest clusters investigated is indicated in Figure 9 where we present results for $C(t)$ computed for S_1 solutes in order to have similar characteristics in the cluster dynamics in equilibrium and nonequilibrium runs.[30] Surprisingly enough, we observe that despite the complexities found in the microscopic mechanisms that drive the overall solvation, the performance of LRT is totally satisfactory for both solvents.

Concluding Remarks

The results presented in this paper show new characteristics for the solvation of large polyatomic probes in polar nanoclusters. At temperatures close to $T = 200$ K, even though the smallest clusters exhibit signs of liquidlike behavior, the solvation is dominated by the trapping in a local free energy minimum, which prevents a uniform solvation of the probe. For the specific case of C-151 attached to clusters containing five solvent molecules, this anisotropy in the solvent structure leads to a preferential solvation of the amino group, in agreement with experimental information.[6,7] However, we found no evidences of preferential solvation of the carbonyl group for either solvent investigated. For electronically excited probes, the solvation presents bimodal characteristics with interconversions between two structures characterized by time scales much larger than those corresponding to the solvent relaxation upon an electronic excitation of the probe. Anisotropies in the solvation structures still remain in larger aggregates and lead to the stabilization of surface/bulklike states of the probe attached to water/methanol clusters. In the dynamical response, the appearance of bulk solvation is reflected into a more clear time scale separation between the initial fast inertial regime and the much slower diffusive mechanism that dominates the long time behavior of the response. Note that in passing from $N_s =$ 10 to 50, the overall characteristic time for methanol clusters increases 1 order of magnitude, whereas for water clusters, τ_s remains practically unchanged. This is not totally unexpected considering the persistence of solute superficial states in the largest water clusters.

The decomposition of the total response in terms of a sum of local contributions from different solute sites shows two interesting features: First, there seems to be no evident correlation between the local change in the electronic distribution of the probe and the magnitude of the local response of the environment. Second, the overall solvent response is the result of different site-contributions that, in certain cases, may exhibit different signs. Nevertheless, it is perhaps due to these cancelative effects that these nonlinearities get suppressed, and still, one finds excellent agreement between the nonequilibrium response and predictions from linear theories.

Summarizing, our simulation results suggest that the overall solvation structure and dynamics at a nanometer scale are strongly influenced by the nature of the spatial charge distribution of the solute probe and the characteristics of the solute−solvent and solvent−solvent interactions. In ionic systems, the solvent density fields in the vicinity of a large solute probe are the result of a complex interplay between these, normally competing, effects and present qualitative differences of difficult prediction.

Acknowledgment. We are grateful to M.S. Skaf for many fruitful discussions and technical assistance. Partial financial support from Fundación Antorchas of Argentina is very much appreciated. D.L. is a staff member of CONICET (Argentina).

Supporting Information Available: Full description of the different solute site coordinates and charges are contained in Table S1. This material is available free of charge as Supporting Information via the Internet at http://pubs.acs.org.

References and Notes

(1) Castleman, A. W.; Keese, R. G. *Chem. Rev.* **1986**, *86*, 589. Castleman, A. W.; Keese, R. G. *Annu. Rev. Phys. Chem.* **1986**, *37*, 525. Castleman, A. W.; Keese, R. G. *Science* **1988**, *241*, 36. Castleman, A. W.; Wei, S. *Annu. Rev. Phys. Chem.* **1994**, *45*, 685.

(2) See, *Physics and Chemistry of Finite Systems: From Clusters to Crystals*; Jena, P., Khana, S. N., Rao, B. K., Eds. Kluwer: Dordrech, The Netherlands, 1992.

(3) See papers in *Small Particles and Inorganic Clusters*; Andersen, H. H., Ed. Springer-Verlag: Berlin, Germany, 1997.

(4) Surface and bulk solvation states have been found in simple halides dissolved in water clusters. For recent studies, see: Jorgensen, W. L.; Severance, D. L. *J. Chem. Phys.* **1993**, *99*, 4233. Dang, L. X.; Smith, D. E. *J. Chem. Phys.* **1993**, *99*, 6950. Perera, L.; Berkowitz, M. L. *J. Chem. Phys.* **1991**, *95*, 1954. Perera, L.; Berkowitz, M. L. *J. Chem. Phys.* **1992**, *96*, 8288. Perera, L.; Berkowitz, M. L. *J. Chem. Phys.* **1993**, *99*, 4236. Tobias, D. J.; Jungwirth, P.; Parrinello, M.; *J. Chem. Phys.* **2001**, *114*, 7036.

(5) Pryor, B. A.; Palmer, P. M.; Andrews, P. M.; Berger, M. B.; Topp, M. R. *J. Phys. Chem. A* **1998**, *102*, 3284.

(6) Palmer, P. M.; Chen, Y.; Topp, M. R. *Chem. Phys. Lett.* **2000**, *318*, 440.

(7) Palmer, P. M.; Chen, Y.; Topp, M. R. *Chem. Phys. Lett.* **2000**, *321*, 62.

(8) Michael, D.; Benjamin, I. *J. Chem. Phys.* **2001**, *114*, 2817.

(9) Nandi, N.; Bagchi, B. *J. Phys. Chem. B* **1997**, *101*, 10954.

(10) Nandi, N.; Bagchi, B.; Pethig, R. *Annu. Rev. Phys. Chem.* **1992**, *43*, 177. Nandi, N.; Bhattacharyya, K.; Bagchi, B. *Chem. Rev.* **2000**, *100*, 2013.

(11) (a) Bagchi, B. *Annu. Rev. Phys. Chem.* **1989**, *40*, 115. (b) Bagchi, B.; Chandra, A. *Adv. Chem. Phys.* **1991**, *80*, 1.

(12) Maroncelli, M. *J. Mol. Liq.* **1993**, *57*, 1.

(13) Maroncelli, M.; Kumar, P. V.; Papazyan, A.; Horng, M. L.; Rosenthal, S. J.; Fleming, G. R. In *Ultrafast Reaction Dynamics and Solvent Effects*; Gaudel, Y., Rossky, P. J., Eds.; American Institute of Physics: New York, 1994.

(14) Stratt, R. M.; Maroncelli, M. *J. Phys. Chem.* **1996**, *100*, 12981.

(15) Fleming, G. R. *Chemical Applications of Ultrafast Spectroscopy*; Oxford University Press: New York, 1986.

(16) Simon, J. D. *Acc. Chem. Res.* **1988**, *21*, 128.

(17) Landayi, B. M. In *Theoretical Methods in Condensed Phase Chemistry*; Schwartz, S. D., Ed.; Kluwer Academic Publishers: Dordrech, The Netherlands, 2000.

(18) Liotard, D. A.; Healy, E. F., Ruiz, J. M.; Dewar, M. J. S. *QCPE Bull.* **1989**, *9*, 123; AMPAC, version 2.1.; Quantum Chemistry Program Exchange program no. 506.

(19) McCarthy, P. K.; Blanchard, G. J. *J. Phys. Chem.* **1993**, *97*, 12205.

(20) Rechthaler, K.; Köhler, G. *Chem. Phys.* **1994**, *189*, 99.

(21) A similar parametrization to that used in this work was implemented by Kumar, P. V.; Maroncelli, M. *J. Chem. Phys.* **1995**, *103*, 3038. Reynolds, L.; Gardecki, J. A.; Frankland, S. J. V.; Horng, M. L.; Maroncelli, M. *J. Phys. Chem.* **1996**, *100*, 10337.

(22) Berendsen, H. J. C.; Postma, J. P. M.; Von Gunsteren, W. F.; Hermans, J. *Intermolecular Forces*; Reidel: Dordrecht, The Netherlands, 1981.

(23) Jorgensen, W. L. *J. Phys. Chem.* **1986**, *90*, 1276.

(24) The characterization of solidlike and liquidlike behaviors depends on the cluster size considered. For small aggregates, liquidlike structures exhibit frequent modifications in their overall intramolecular connectivity. On the other hand, in liquidlike larger clusters, water molecules exhibit diffusive behavior manifested by an intermediate linear time dependence in their root-mean-square displacements.

(25) Allen, M. P.; Tildesley, D. J. *Computer Simulations of Liquids*; Clarendon Press: Oxford, U.K., 1987.

(26) Ryckaert, J.-P.; Ciccotti, G.; Berendsen, H. J. C. *J. Comput. Phys.* **1977**, *23*, 327.

(27) Chandler, D. *An Introduction to Modern Statistical Mechanics*; Oxford University Press: New York, 1987; Chapter 8.

(28) Ladanyi, B.; Stratt, R. M. *J. Phys. Chem.* **1995**, *99*, 2502.

(29) Fonseca, T.; Ladanyi, B. M. *J. Chem. Phys.* **1991**, *2116*, 95

(30) Similar agreement between $C(t)$ and $S(t)$ was found in different test runs performed on systems with S_0 solutes.